# Controlling Catalyst Phase Selectivity in Complex Mixtures with Amphiphilic Janus Particles

Benjamin Greydanus, Daniel K. Schwartz, and J. Will Medlin

*Dept. of Chemical and Biological Engineering, University of Colorado, Boulder, CO*

*Supporting Information*

**ABSTRACT:** Amphiphilic Janus particles with catalyst selectively loaded on either the hydrophobic or hydrophilic region are promising candidates for efficient and phase-selective interfacial catalysis. Here, we report the synthesis and characterization of Janus silica particles with a hydrophilic silica domain and a silane-modified hydrophobic domain produced via a wax masking technique. Palladium nanoparticles were regioselectively deposited on the hydrophobic side and the phase selectivity of the catalytic Janus particles was established through kinetic studies of benzyl alcohol hydrodeoxygenation (HDO). These studies indicated that the hydrophobic moiety provided nearly 100x the catalytic activity as the hydrophilic side for benzyl alcohol HDO. The reactivity was linked to the anisotropic catalyst design through microscopy of the particles. The catalysts were used to achieve phase-specific compartmentalized hydrogenation and selective in-situ catalytic degradation of a model oily pollutant in a complex oil/water mixture.

KEYWORDS: *Janus particles, catalytic Janus particles, Pickering emulsion, interfacial catalysis, selective catalysis*

## 1. INTRODUCTION

Complex mixtures of oil and water are ubiquitous in industry with applications ranging from biomass conversion to wastewater remediation.[1,2] However, controlling selective catalytic transformations in these complex mixtures remains a challenge. A potentially powerful method for combining phase selectivity, emulsion stability, and ease of product recovery incorporates a heterogeneous catalyst with two distinct chemical surfaces and a catalytic metal selectively deposited on one surface.[3] Known as Janus particles, these surface-anisotropic particles have attracted widespread attention over the last decade with applications including solid surfactants, self-propelled motors, and self-assembly.[4–8] Amphiphilic Janus particles preferentially assemble at the oil/water interface, enhancing emulsion stability and greatly increasing the liquid-liquid interfacial area.[9,10] It is generally accepted that Janus particles with a dominant hydrophilic domain stabilize oil-in-water (o/w) emulsions and particles with a dominant hydrophobic domain stabilize water-in-oil (w/o) emulsions.[11] In its most energetically favored orientation, an amphiphilic particle pinned at the interface exposes each domain to its preferred phase.[12] While the particle likely still retains some degree of rotational freedom, the amphiphilic surface chemistry should heavily bias these rotational states towards the favored orientation.[13–15] Thus, a catalyst selectively loaded on the hydrophobic region should predominately be exposed to the oil phase and should therefore overwhelmingly catalyze transformations of oil

soluble species. Solid particles can be easily separated from the reaction mixture, breaking the emulsion and potentially facilitating recovery of products and catalysts.[16] Since catalytic Janus particles marry facile product recovery, emulsion stability, and catalytic phase selectively, their utility is especially apparent for selective catalytic treatment of complex mixtures without the need for separations.

In previous work, Janus particles with varying architectures have been loaded with metals and shown to act as efficient interfacial catalysts. Crossley et al. functionalized silica with carbon nanotubes to create amphiphilic hybrid particles that were subsequently loaded with palladium.[17] These hybrids showed excellent activity and reasonable phase selectivity, as the palladium apparently deposited preferentially on the hydrophilic silica moiety. The Resasco group further expanded their library of interfacial catalysts with magnesium oxide/carbon nanotube hybrids loaded with palladium, which was found to deposit more favorably on the hydrophobic nanotubes, thus promoting catalytic reactions in the nonpolar phase. These amphiphilic hybrids were used to catalyze several reactions, including Fischer–Tropsch synthesis and sub-surface enhanced oil recovery.[18,19] "Hairy" Janus particles loaded with catalyst have also been reported in the literature. By growing a hydrophobic and hydrophilic polymer on opposite ends of a silica core, Kirillova et al. developed amphiphilic particles with proposed uses in biofilm protection and icing/deicing.[20] Furthermore, it was

demonstrated that gold and silver nanoparticles could be immobilized in the polymer, creating a catalytic Janus particle.[21] Other exotic catalytic Janus materials have also been reported, including hollow Janus microcapsules,[22] Janus sheets with tethered acid or basic functionality,[23] and "Snowman" catalytic Janus particles with Au largely loaded on the hydrophobic sphere.[24] Further, Cho et al. described the synthesis and applications of anisotropic particles with site-specific deposition of magnetic nanoparticles.[25] These Janus particles were then further unselectively decorated with Pd nanoparticles and their catalytic utility was proven through a variety of organic reactions. The most comprehensive example of phase-selective catalytic Janus particles involved the reported synthesis of very small (7 nm) silica Janus particles using an amine-terminated silane as the modifier.[3] Pd was loaded on the hydrophobic side and, in a biphasic system containing oil-soluble benzaldehyde and water-soluble glutaraldehyde, the catalysts showed selective hydrogenation of benzaldehyde.

Here, we synthesized 500 nm Janus silica particles and selectively loaded catalytic palladium nanoparticles onto the hydrophobic particle moiety. By using 500 nm particles, the Janus character of the metal deposition was more apparent than with Janus nanoparticles, and, as "flipping" and mis-orientation of small Janus particles at the interface has been previously reported,[26,27] a stronger biasing of particle rotation towards the thermodynamically favored orientation was potentially asserted. The phase selectivity of these particles toward the oil phase was probed through the kinetics of batch reactions. The observed reaction selectivity (which was compared to uniform catalytic particles as a control) was linked to the catalyst topography through microscopy. The synthesized catalysts were also used for phase-selective compartmentalized hydrogenation and in-situ catalytic degradation of a model pollutant.

## 2. EXPERIMENTAL SECTION

### 2.1. Materials.

Hexadecyltrimethylammonium bromide (CTAB, ≥99%), paraffin wax (mp ≥65 °C), (3-aminopropyl)triethoxysilane (APTES) (99%), palladium(II) nitrate dihydrate, benzaldehyde (≥99%), benzyl alcohol (99.8%), vanillyl alcohol (≥98%), 2-methoxy-4-methyl-phenol (p-creosol, ≥98%), toluene ≥99.5%), decahydronaphthalene(decalin, mixture of cis +trans, ≥99%), heptadecane (99%), dodecane (≥99%), and Sudan III were purchased from Sigma-Aldrich. Isooctane (99%) and high-performance liquid chromatography (HPLC)-grade water (≥99.9%) were purchased from Fisher Scientific. Chloroform (≥99.8%, Macron), methanol (≥99.8%, VWR), ammonium hydroxide (70% w/w, PubChem), silica spheres (500 nm diameter, non-porous, SA 6.02 ± 0.07 m$^2$/g, Alfa Aesar), and Methyl Blue (MP Biomedicals) were purchased from suppliers as indicated. Prepurified nitrogen and ultra-high-purity H$_2$ were obtained from Airgas.

### 2.2. Catalyst Preparation and Characterization.

Chemical anisotropy was introduced onto 500 nm silica spheres using a previously described wax masking technique (Figure S1).[28,29] Briefly, the silica spheres were dispersed in deionized water and CTAB was added to partially hydrophobize the silica surface. The amount of CTAB was set to create a 0.1 mM solution, a concentration observed to result in a high-quality silica monolayer. After stirring for 30 minutes, the solution was heated to 75 °C, 5.4 g of paraffin wax was added and the solution was emulsified via vigorous mechanical stirring for 1 hour. The solution was then cooled to room temperature and the solid wax droplets were collected via filtration. The presence of the silica spheres embedded in the wax surface was characterized using a Hitachi SU3500 Scanning Electron Microscope. The wax droplets were then redispersed in a 10mM solution of (3-aminopropyl)triethoxy-silane (APTES) in methanol, water, and ammonia (100 mL, 7 mL, and 7 mL, respectively). While APTES is prone to polymerization in the presence of water and ammonia, the large excess of silane relative to the particle surface area likely ensured a high degree of surface silanization. The APTES surface modification process was allowed to proceed at room

temperature overnight with the silane grafting to the exposed silica surface. APTES provided a facile method to functionally impart hydrophobicity to the particles under the reaction conditions. It is important to note that APTES is known to undergo hydrolytic degradation over long times with studies indicating a >50% loss in APTES content after several days immersed in water.[30] Thus, while APTES was expected to provide a coating suitable to create hydrophobic character over the reaction times (<60 min) employed in the current study, future work may benefit from the use of other amino silanes, especially those with longer chain lengths where issues with self-catalyzed hydrolysis have been shown to be mitigated.[31,32] The wax droplets were again recovered via filtration and rinsed with methanol to remove any weakly attached silane. The wax was then dissolved using chloroform, releasing the Janus silica particles with two distinct chemical surfaces: bare hydrophilic silica and hydrophobic organosilane. The surface silanization of the particles was characterized through diffuse reflectance infrared Fourier transform spectroscopy (DRIFTS) using a Thermo Scientific Nicolet 6700.

Catalytic functionality was introduced via a wet deposition method.[3] After silane modification, the particles, while still embedded in wax, were stirred in a methanolic solution of $Pd(NO_3)_2$ for 2 hours to seed metal clusters on the exposed side of the silica. Depositing the metal while the silica was embedded in the wax helped ensure that the metal nanoparticles were selectively seeded onto only the hydrophobic, silanized silica surface. Evidence of the neighboring silica particles in the monolayer was observed in the metal deposition, with bare metal-free patches on particles likely corresponding to areas in physical contact with nearby silica particles and relatively higher degrees of metal functionalization on "top" of the particles where minimal steric barriers to metal deposition were expected. The metal-seeded particles in wax were then dried under vacuum for at least 2 days before the wax was dissolved using chloroform. The released particles were rinsed three times with chloroform and twice with methanol and then dried overnight at 100 °C. Finally, the particles were calcined at 200 °C in air for two

hours to convert the seeded Pd clusters to metallic nanoparticles (NPs).

As a control case, uniform particles with Pd NPs unselectively deposited across the entire particle surface were prepared by dispersing 0.5 g of cleaned silica particles (500 nm) in a solution of methanol, water, and ammonia (100 mL, 7 mL, and 7 mL, respectively). The particles were stirred for 1 hour, then 0.5 mL of APTES was added and the solution was stirred overnight. The particles were separated via centrifugation, rinsed four times with methanol, then dried overnight at 100 °C. The dried particles with APTES unselectively grafted onto the entire particle were stirred in a solution of $Pd(NO_3)_2$ in methanol for 2 hours to uniformly seed metal clusters onto the particle. These metal-loaded particles were then dried under vacuum for at least 2 days before being dried overnight at 100 °C and finally calcined in air at 200 °C. The metal deposition procedures for the Janus and uniform catalysts were functionally identical, differing only by the wax dissolution step, and the final electronic states of the metal nanoparticles were expected to be similar between the catalyst types.

The metal-decorated Janus particles and uniform particles were characterized using a Tecnai ST20 TEM operating at 200 kV. Samples of the particles were sonicated in a solution of water and methanol and a small aliquot was drop-cast onto a holey carbon-coated copper grid (Ted Pella) and dried under vacuum for at least 4 hours before TEM analysis.

Colormetric analysis of dye degradation was performed using a Cary Series UV-Vis Spectrophotometer (Agilent).

The metal loading of the synthesized catalysts was characterized using ICP-MS. Measured amounts of the catalysts were dispersed in a solution of aqua regia to dissolve the loaded Pd. (**Caution! Aqua regia solutions are extremely corrosive and should be handled with caution**.) A calibration curve of standard Pd solutions was also prepared using aqua regia and $PdCl_2$. All solutions were then diluted into a solution of 1% nitric acid in HPLC water and analyzed using a Thermo Element2 HR-ICPMS.

## 2.3. Catalytic Reactions

All biphasic hydrogenation reactions were run using a 100 mL Parr semibatch reactor operating at 50 °C and 200 psi $H_2$ for 1 hour. The reaction mixture consisted of 16 mL of water and 16 mL of oil (decalin, heptadecane, or isooctane), 160 μL (0.04 M) of reactant (benzaldehyde, benzyl alcohol, or vanillyl alcohol), 0.01 mmol Pd catalyst, 1 mL of methanol (aqueous phase internal standard), and 1 mL of dodecane (organic phase internal standard). The biphasic reaction was mixture was emulsified through a rapid stirring rate of 1200 rpm and six aliquots (average volume 0.75-1.5 mL) were taken from the reactor during the hour-long reaction. The aliquots were filtered to remove the catalyst and, as the catalyst was expected to be uniformly distributed in the reaction mixture due to the rapid stirring rate, simultaneous sampling of the reaction mixture and catalyst was expected to result in a constant ratio of catalyst to reaction mixture in the reactor.[33] After filtration, the organic and aqueous phases of each aliquot were separated and each phase was analyzed using an Agilent 7890A gas chromatograph equipped with a flame ionization detector and Agilent HP-5 capillary column. To assess the concentration of each analyte, the observed GC responses were compared to a set of standard solutions prepared with similar concentrations to those under reaction conditions. Due to the constant temperature and vigorous stirring of the reaction mixture, the reactant partition coefficient was observed to be constant throughout the hour-long reaction (Figure S2) and kinetic analyses and rates were calculated using the summed analyte concentrations from both phases. Reported error bars were computed from replicate reactions.

## 2.4. Kinetic Fitting

First-order fitting of benzyl alcohol hydrodeoxygenation (HDO) reactions in biphasic mixtures gave an effective rate constant ($k_{eff}$) for the combined reaction in both phases. To elucidate the activity associated with each specific face of the particle (oil-facing and water-facing), the benzyl alcohol reaction was run using three different solvents as the oil phase (decalin, heptadecane, and isooctane), since the reactants and products are known to have different affinities (i.e. partition coefficients) in these solvents. Specifically, the solubility of benzyl alcohol in the oil phase ($\chi$) differs for the different solvents (Figure S2). The reactions were observed to be first-order with respect to benzyl alcohol concentration, leading to the development of a first-order rate expression (eqn 1) to model the relative contributions of the oil and water phases to the overall observed rate.

$$\frac{dC_{Benzyl\ Alcohol}}{dt} = k_{eff} C_{Benzyl\ alcohol} = k_{Oil}\ \chi\ C_{Benzyl\ alcohol} + k_{Water}\ (1-\chi)\ C_{Benzyl\ alcohol} \quad (1)$$

The observed first-order rate constants were attributed to external diffusion of the reactant[34] as determined by classical tests for transport limitations (see the Supporting information for details). The kinetic parameters $k_{oil}$ and $k_{water}$ were extracted from the reaction data by fitting the measured $k_{eff}$ values from different oil phases with the respective values of $\chi$ (eqn 1) as inputs. Error bars were computed using Matlab by simultaneously fitting replicates of reactions in each oil phase.

## 3. RESULTS AND DISCUSSION

### 3.1 Synthesis of Janus Catalysts.

SEM imaging of solid wax droplets showed the silica particles embedded in the wax surface in near-monolayer fashion (Figure 1) with occasional defective regions exhibiting small aggregates and/or vacancies.
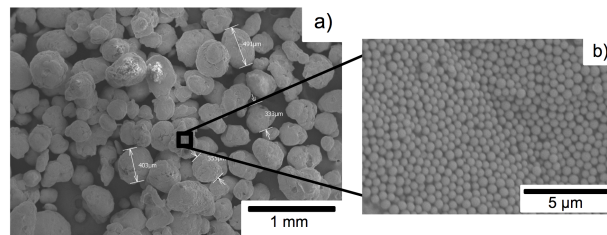


**Figure 1.** Representative SEM images of solidified wax droplets with embedded silica particles. **a)** Lower magnification image of solid wax droplets; **b)** silica particle monolayer embedded in wax droplet surface.

SEM imaging after silane deposition and metal deposition confirmed the presence of silica particles embedded in the wax (Figure S3). Further, it appeared that the majority of silica embedded was from the monolayer as opposed to the above-

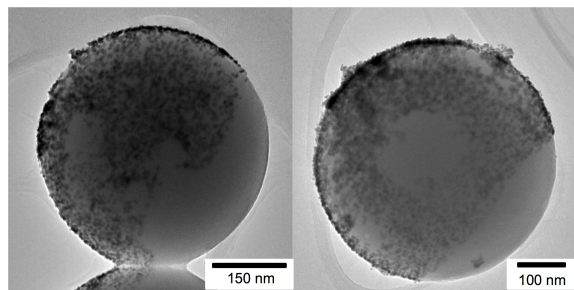surface clusters which likely detached in the dep-



**Figure 2.** Representative TEM micrographs of metal-loaded particles exhibiting Janus character.

osition processes and rinsing.[35] After dissolution of the wax, DRIFT spectra showed the presence of the APTES modifier on the silica through characteristic C-N and C-H stretches (Figure S4). TEM micrographs confirmed the presence of Pd NPs on the catalyst surface as well as the asymmetric Janus nature of the metal deposition (Figure 2). While particles exhibiting Janus character were readily observable, significant heterogeneity in Pd NP arrangement was observed, with some particles exhibiting little Pd and others appearing to be nearly homogenously modified with Pd NPs. As expected, the uniform catalyst particles were observed to be unselectively decorated with Pd NPs and similar Pd NP size distributions were observed between the catalyst types: 4.6±0.7 nm for Janus and 4.0±1.0 nm for uniform. We also estimated the Pd dispersion by comparing benzaldehyde hydrogenation rates to those measured over a standard catalyst (details in Supporting Information) and estimated dispersions for the Janus (15%) and uniform (18%) catalysts that are consistent with these particle sizes. Additional representative images of these Janus particles (Figure S5) and the uniform catalyst particles (Figure S6) are included in the supporting information.

## 3.2 Probing Phase Selectivity with Kinetic Parameters

To systematically probe the phase selectivity of the Janus catalysts, biphasic oil and water reactor studies were performed using benzyl alcohol as the reactant. As discussed above, reactions were carried out in a regime for which external mass transfer limitation was determined to be rate-limiting. For both the Janus catalyst (Pd selectively loaded on the hydrophobic side) and the uniform catalyst (Pd on both sides), stable three-phase reaction mixtures were observed with clear oil and water phases separated by a w/o emulsion phase (Figure S7). The observed formation of w/o emulsions (characteristic of predominantly hydrophobic particles) provided further evidence of successful hydrophobic silane functionalization of both particles. Further, no dispersed particles of either type were observed in the oil or water phases, indicating both particle types were adsorbed to the emulsion interface. Apparently identical emulsions were observed post-reaction, suggesting that, despite the potential loss of APTES-functionalization,[30] the surface modification was robust enough to functionally provide hydrophobic character throughout the reaction period. The three-phase contact angle of both particle types at the emulsion interface was estimated to be 94±3° and 105±1° for Janus and uniform, respectively (Figure S8 and experimental details in the Supporting Information). To probe whether the anisotropic nature of the Janus particles was indeed biasing the particles to favor the proposed reaction orientation, i.e. metal-loaded APTES surface facing the hydrophobic phase and bare silica surface facing the hydrophilic phase, three oil-phase solvents were used: decalin, heptadecane, and isooctane. The solubility of benzyl alcohol in the oil phase systematically decreased from decalin to heptadecane to isooctane, with $\chi=0.19, 0.15, 0.12$, respectively. Importantly, as the solubility of benzyl alcohol in the oil phase was reduced, the $k_{eff}$ value similarly decreased over the Janus catalysts (Figure 3), consistent with the hypothesis that the Janus catalyst selectively converted oil-soluble species. Over the uniform catalyst, the $k_{eff}$ values were largely insensitive to changes in the oil phase solvent, suggesting that the uniform particles were similarly adsorbed at the oil/water interface regardless of the specific choice of oil.[36] Further, the relative insensitivity in $k_{eff}$ of the uniform catalyst to the changing oil phase (decalin to heptadecane to isooctane) suggested that the decreasing oil-phase reactant concentration indeed correlated with the observed decrease in $k_{eff}$ for the Janus catalysts due to selective oil-phase activity as opposed to an intrinsic solvent-mediated rate suppression.[37]
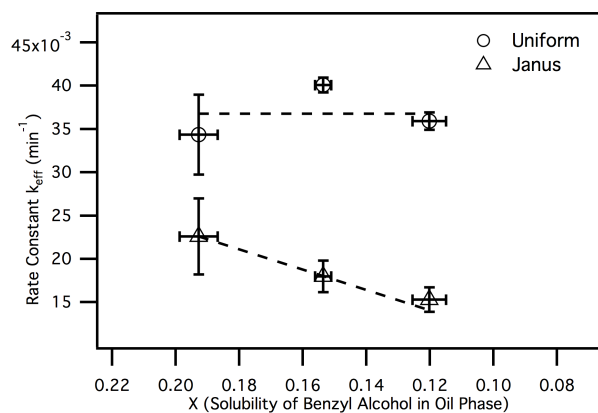
5

**Figure 3.** $k_{eff}$ for benzyl alcohol HDO in biphasic reaction mixtures with different oil phases for Janus and uniform catalysts. Reaction conditions: 0.045 M benzyl alcohol, 0.01 mmol Pd catalyst, 16 mL of water and 16 mL of oil (decalin, heptadecane, or isooctane), 1 mL of methanol and 1 mL of dodecane (internal standards), 50 °C, 200 psi H₂, and stirring at 1200rpm. Dashed lines show expected behavior for the "ideal cases," i.e. equal oil and water activity for the uniform (value: average of three observed $k_{eff}$) and perfect oil-phase selectivity for Janus catalysts (value: observed $k_{eff}$ in decalin), respectively.

The observed $k_{eff}$ values for benzyl alcohol HDO over the Janus catalyst (Figure 3) were fitted to a first-order model (eqn 1) to extract $k_{oil}$ and $k_{water}$, the rate constants for the reaction on the oil-facing particle face and the reaction on the water-facing side. As these $k$ values are directly proportional to the number of active metal sites on each respective side, comparing the relative magnitudes is an effective way to measure the anisotropy of the metal deposition on the catalyst. As shown in Table 1, the value of $k_{oil}$ for the Janus catalyst was 0.11 ± 0.03, nearly 100x larger than $k_{water}$ 0.001 ± 0.006, consistent with the goal of creating a strongly oil-selective interfacial catalyst. Over the uniform catalyst, $k_{oil}$ and $k_{water}$ were equal in magnitude within experimental uncertainty (0.04± 0.03 and 0.038 ± 0.006, respectively), as expected for an unselectively prepared interfacial catalyst with metal on both the oil and water-facing moieties. Since the majority of Pd was segregated on the hydrophobic side in the Janus catalyst, the Janus $k_{oil}$ was larger than the uniform $k_{oil}$ where approximately the same total amount of Pd was distributed across the entire particle surface.

## Table 1. Apparent Oil and Water Kinetic Parameters (min⁻¹)

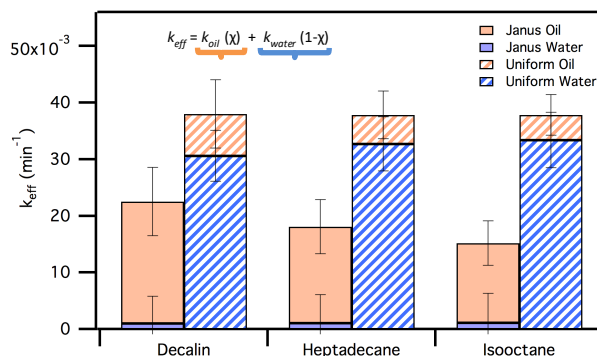| Catalyst | $k_{oil}$ | $k_{water}$ |
|----------|-----------|-------------|
| Janus | 0.11 ± 0.03 | 0.001 ± 0.006 |
| Uniform | 0.04 ± 0.03 | 0.038 ± 0.006 |



**Figure 4.** Relative contributions of $k_{oil}$ and $k_{water}$ to $k_{eff}$ for benzyl alcohol HDO in biphasic reaction mixtures with different oil phases for both Janus and uniform catalysts. Reaction conditions: 0.045 M benzyl alcohol, 0.01 mmol Pd catalyst, 16 mL of water and 16 mL of oil (decalin, heptadecane, or isooctane), 1 mL of methanol and 1 mL of dodecane (internal standards), 50 °C, 200 psi H₂, and stirring at 1200 rpm.

Analyzing the relative contributions of $k_{oil}$ and $k_{water}$ to the overall observed $k_{eff}$ (Figure 4) demonstrated a profound difference between the observed activity of uniform and Janus catalyst. For the uniform catalyst, due to the near-parity between $k_{oil}$ and $k_{water}$ (Table 1), the relative activity in each phase was determined simply by the partitioning of the reactant between the phases. Thus, the higher solubility of benzyl alcohol in the water phase resulted in a similarly larger contribution to the overall activity. For the Janus catalyst, however, the observed activity was dominated by the contribution from the oil side with minimal reactivity of the water-soluble benzyl alcohol, despite the increased solubility in the water phase. These kinetic parameters provided compelling support for the phase-selectivity of the Janus catalysts, demonstrating that carefully designed spatial modification of the particles can have profound impacts on selective biphasic processes. In particular, for an unselective interfacial catalyst, in the absence of severe solvent effects, relative activity in each phase was regulated simply by the relative reactant solubility. However, by segregating the

6

catalytic metal to one side of an amphiphilic interfacial catalyst, one can break this paradigm and achieve control over relative activity with the vast majority of observed activity coming from the phase with significant reduced reactant solubility.

### 3.3 Testing Model Validity with Vanillyl Alcohol HDO

The validity of the calculated kinetic parameters was tested in hydrogenation reactions using vanillyl alcohol as the reactant (Table 2). In a water/decalin mixture, vanillyl alcohol has negligible partitioning into the oil phase[38] and thus is an effective tool to probe the robustness of the calculated $k_{water}$.

**Table 2. $k_{water}$ Values Extracted from Model and Vanillyl Alcohol HDO**

| Catalyst | Model $k_{water}$ | Observed $k_{water}$ |
|---|---|---|
| Janus | $0.001 \pm 0.006$ | $0.002 \pm 0.001$ |
| Uniform | $0.0038 \pm 0.006$ | $0.04 \pm 0.03$ |

Reaction conditions: 0.04 M vanillyl alcohol, 0.01 mmol of Pd catalyst, 16 mL of water and 16 mL of decalin, 1 mL of methanol and 1 mL of hexadecane (internal standards), 50 °C, 200 psi $H_2$, and stirring at 1200 rpm. Reaction profiles shown in supporting info (Figure S9).

As shown in Table 2, the experimentally observed $k$ values for both the Janus catalyst and the uniform catalyst showed good agreement with the calculated $k_{water}$ values, supporting the validity of the kinetic parameters extracted from the benzyl alcohol experiments (Table 1).

### 3.4 Compartmentalized Hydrogenation of Benzaldehyde

The Janus catalyst and uniform catalyst were employed for the hydrogenation of benzaldehyde to illustrate the utility of the Janus catalyst towards facilitating phase-selective compartmentalized reactions. Compartmentalized reactions are of continued interest due to their promise of combining metal chemocatalytic reactions and biocatalytic processes for one-pot multicatalytic cascade reactions.[39–41] Biocatalysts often require aqueous conditions and combining biocatalysts with transition-metal catalysts frequently results in mutual inactivation,[42] limiting the utility of such a system for multicatalytic processing of an oily reactant.

However, by segregating the chemocatalyst to the oil phase and the biological catalyst to the water phase, a cascade reaction scheme can result with the chemocatalyst converting the oily reactant to a more water-soluble intermediate than further reacts with the biocatalyst. Performing such a cascade in emulsion conditions is attractive with drastically reduced barriers toward mass-transfer between the phases compared to non-emulsion conditions.[10]
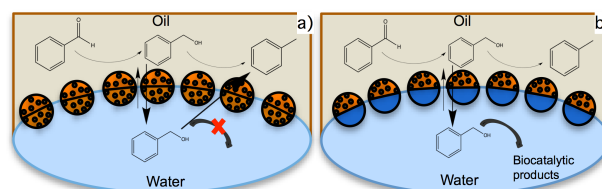


**Figure 5.** Hypothesized reaction scheme of compartmentalized cascade benzaldehyde hydrogenation/HDO in biphasic conditions catalyzed by a) Uniform catalyst and b) Janus catalyst.

Benzaldehyde hydrogenation is a particularly good candidate for compartmentalization since the benzaldehyde reactant is oil-soluble, the intermediate benzyl alcohol is predominantly water-soluble, and the final product toluene is very oil-soluble. Over an oil-phase selective catalyst, one would expect rapid conversion of benzaldehyde to benzyl alcohol (Figure 5b). The benzyl alcohol produced would predominantly partition into the water phase with limited continued chemocatalytic conversion to toluene, opening the possibility for a cascade reaction via a water-soluble biocatalyst. Further, by segregating the Pd to the oil-facing side, we propose issues with severe Pd-induced inhibition of enzymes and other biological catalysts are mitigated.[43,44] Over a uniform catalyst with catalytic centers on both the oil and water-facing moieties, similar conversion of benzaldehyde is expected. However, increased conversion to toluene would be expected since the water-soluble benzyl alcohol would continue to react with water-facing Pd nanoparticles (Figure 5a). The reduced sequestration of benzyl alcohol over the uniform catalyst would limit the efficacy of a water-soluble biological catalyst while also exposing potentially toxic metal sites to the biocatalyst.

Indeed, rapid benzaldehyde conversion to benzyl alcohol was observed over the course of the

7

reaction with the uniform and Janus catalysts (Table S2). As shown in Figure 6, the Janus catalyst displayed significantly higher selectivity towards benzyl alcohol than toluene compared to the uniform catalyst at similar benzaldehyde conversions.
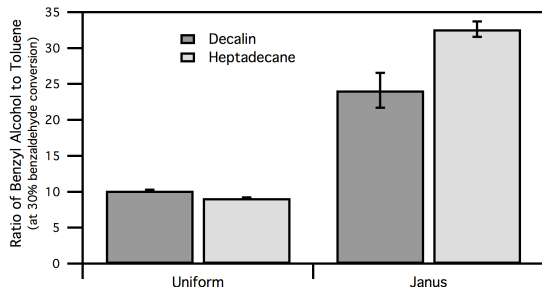


**Figure 6.** Selectivity towards benzyl alcohol intermediate produced via compartmentalized benzaldehyde hydrogenation over the uniform and Janus catalysts. Reaction conditions: 0.05 M benzaldehyde, 0.01 mmol Pd catalyst, 16 mL of water and 16 mL of decalin (solvents), 1 mL of methanol and 1 mL of dodecane (internal standards), 50 °C, 200 psi $H_2$, and stirring at 1200 rpm.

This higher selectivity was attributed to differing rates between the catalysts for benzyl alcohol HDO to form the series product toluene. Over the uniform catalyst, the predominantly water-soluble benzyl alcohol was hydrodeoxygenated in a reaction hypothesized to be occurring on both the water and oil-facing sides of the particle (Figure 5a). In the Janus case, only the small oil-soluble portion of benzyl alcohol could react with the oil-facing sites, leading to a suppression of benzyl alcohol consumption compared to the uniform case and consequently a higher ratio of benzyl alcohol to toluene. Changing the oil phase from decalin to heptadecane (and thereby decreasing the solubility of benzyl alcohol in the oil phase) enhanced the sequestration of water-soluble intermediates over the Janus catalyst. In reactions with heptadecane as the oil phase (Figure 6), selectivity towards benzyl alcohol was relatively unchanged over the uniform catalyst compared with decalin and increased over the Janus catalyst, consistent with the hypothesized sequestration of water-soluble intermediates via suppressed water-phase activity over the Janus catalyst compared to the uniform catalyst. The impact of these varying selectivities on the final sequestration of benzyl alcohol is profound: after 1 hour, >10x more benzyl alcohol remained over the Janus catalyst compared to the uniform catalyst in decalin and some 15x more benzyl alcohol was preserved using heptadecane as the oil phase (Figure S10).

Various biocatalytic processes are known to act on benzyl alcohol and other aromatic alcohols[45], suggesting the utility of Janus catalysts for facilitating these reactions via a compartmentalized cascade reaction starting with benzaldehyde. Further, one can envision an alternative cascade process in an emulsion stabilized by Janus catalyst particles where a water-soluble reactant is biologically converted to form a more lipophilic intermediate that then partitions to the oil phase and continues to react with the oil-facing metal sites.

### 3.5 In-situ Pollutant Degradation

The phase-selective catalytic activity of the synthesized Janus catalysts was further extended to a different practical application involving the in-situ catalytic degradation of an oil-soluble azo dye. Difficult to biodegrade and toxic even at very low concentrations, azo dyes are ubiquitous industrial pollutants.[46] Reductive catalytic degradation over heterogeneous catalysts has been shown to effectively decolorize azo dye solutions through destruction of the –N=N— azo bond.[47] However, since many less toxic water-soluble dyes are similarly sensitive to reductive degradation, selective in-situ degradation of these azo dyes in a complex industrial mixture is challenging with an unselective catalyst. To demonstrate the phase selectivity of the Janus catalyst for this application, the Janus catalyst and uniform catalyst were used to stabilize a complex oil/water mixture containing both an oil-soluble azo dye (Sudan III) and the more environmentally benign water-soluble dye (Methyl Blue).
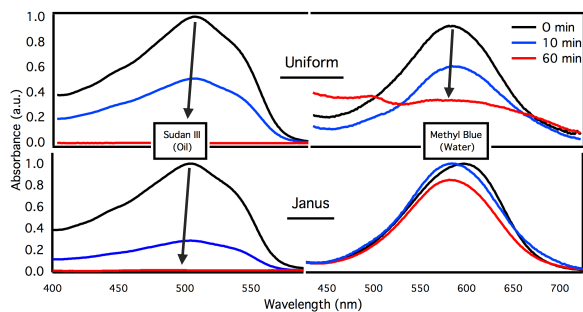
**Figure 7.** Time-dependent UV-Vis spectra for Sudan III and Methyl Blue degradation in biphasic reaction conditions catalyzed by the Uniform catalyst and Janus catalyst. Reaction conditions: 5 mM Sudan III, 5 mM Methyl Blue, 0.01 mmol Pd catalyst, 16 mL of water and 16 mL of decalin (solvents), 22 °C, 200 psi $H_2$, and stirring at 1200 rpm. Control case (no catalyst) shown in Figure S11.

In the emulsion conditions stabilized by the unselective uniform catalyst, both dye solutions were rapidly decolorized (Figure 7) with 99% conversion of Sudan III and 66% conversion of Methyl Blue. Over the Janus catalyst, only the oil-soluble azo dye was appreciably degraded over the reaction period (99% conversion of Sudan III and 15% Methyl Blue conversion). The controlled reactivity of the Janus catalyst was further supported as control reactions with no catalyst loaded also resulted in nearly 10% Methyl Blue conversion (Figure S11), suggesting the water-phase activity observed over the Janus catalyst was also partly due to other non-catalytic processes, e.g., thermal degradation. The rapid and selective degradation of the harmful azo dye Sudan III in a complex mixture showcased the highly phase-specific activity of Pd-bearing Janus catalysts for in-situ pollutant remediation.

## 4. CONCLUSION

In this study, we reported the synthesis and characterization of silica Janus particles with well-defined phase selectivity towards oil-soluble species. Systematic kinetic studies of benzyl alcohol hydrodeoxygenation using various oil phase solvents demonstrated that the $k_{oil}$ of the Janus catalysts was approximately two orders of magnitude larger than $k_{water}$. These kinetic results were directly linked to the anisotropic deposition of Pd NPs on the hydrophobic side through microscopy of the particles. Practical applications of the phase-selective Janus catalysts were shown with compartmentalized benzaldehyde processing and the phase selective in-situ degradation of a lipophilic azo dye pollutant.

## ASSOCIATED CONTENT

**Supporting Information**

The Supporting Information is available free of charge

> Additional reaction and characterization data as described in text

## AUTHOR INFORMATION

**Corresponding Author**

*E-mail: Will.Medlin@colorado.edu.

**ORCID**

J. Will Medlin: 0000-0003-2404-2443

**Notes**

The authors declare no competing financial interest.

# REFERENCES

(1) Román-Leshkov, Y.; Chheda, J. N.; Dumesic, J. A. Phase Modifiers Promote Efficient Production of Hydroxymethylfurfural from Fructose. *Science (80).* **2006**, *312* (5782), 1933–1937.

(2) de Tuesta, J. L. D.; Machado, B. F.; Serp, P.; Silva, A. M. T.; Faria, J. L.; Gomes, H. T. Janus Amphiphilic Carbon Nanotubes as Pickering Interfacial Catalysts for the Treatment of Oily Wastewater by Selective Oxidation with Hydrogen Peroxide. *Catal. Today* **2019**, No. July, 1–11.

(3) Faria, J.; Ruiz, M. P.; Resasco, D. E. Phase-Selective Catalysis in Emulsions Stabilized by Janus Silica-Nanoparticles. *Adv. Synth. Catal.* **2010**, *352* (14–15), 2359–2364.

(4) de Gennes, P. G. Soft Matter Soft Matter. *Rev. Mod. Phys.* **2013**, *64* (3), 6545–6563.

(5) Poggi, E.; Gohy, J.-F. Janus Particles: From Synthesis to Application. *Colloid Polym. Sci.* **2017**, 2083–2108.

(6) Walther, A.; Müller, A. H. E. Janus Particles: Synthesis, Self-Assembly, Physical Properties, and Applications. *Chem. Rev.* **2013**, *113* (7), 5194–5261.

(7) Ebbens, S. J.; Howse, J. R. In Pursuit of Propulsion at the Nanoscale. *Soft Matter* **2010**, *6* (4), 726–738.

(8) Ye, Y.; Luan, J.; Wang, M.; Chen, Y.; Wilson, D. A.; Peng, F.; Tu, Y. Fabrication of Self-Propelled Micro- and Nanomotors Based on Janus Structures. *Chem. - A Eur. J.* **2019**, 8663–8680.

(9) Binks, B. P.; Fletcher, P. D. I. Particles Adsorbed at the Oil-Water Interface: A Theoretical Comparison between Spheres of Uniform Wettability and "Janus" Particles. *Langmuir* **2001**, *17* (16), 4708–4710.

(10) Chevalier, Y.; Bolzinger, M. A. Emulsions Stabilized with Solid Nanoparticles: Pickering Emulsions. *Colloids Surfaces A Physicochem. Eng. Asp.* **2013**, *439*, 23–34.

(11) Lan, Y.; Choi, J.; Li, H.; Jia, Y.; Huang, R.; Stebe, K. J.; Lee, D. Janus Particles with Varying Configurations for Emulsion Stabilization. *Ind. Eng. Chem. Res.* **2019**.

(12) Bradley, L. C.; Chen, W. H.; Stebe, K. J.; Lee, D. Janus and Patchy Colloids at Fluid Interfaces. *Curr. Opin. Colloid Interface Sci.* **2017**, *30*, 25–33.

(13) Gao, H. M.; Lu, Z. Y.; Liu, H.; Sun, Z. Y.; An, L. J. Orientation and Surface Activity of Janus Particles at Fluid-Fluid Interfaces. *J. Chem. Phys.* **2014**, *141* (13).

(14) Park, B. J.; Choi, C. H.; Kang, S. M.; Tettey, K. E.; Lee, C. S.; Lee, D. Geometrically and Chemically Anisotropic Particles at an Oil-Water Interface. *Soft Matter* **2013**, *9* (12), 3383–3388.

(15) Fan, H.; Resasco, D. E.; Striolo, A. Amphiphilic Silica Nanoparticles at the Decane-Water Interface: Insights from Atomistic Simulations. *Langmuir* **2011**, *27* (9), 5264–5274.

(16) Wu, Z.; Li, L.; Liao, T.; Chen, X.; Jiang, W.; Luo, W.; Yang, J.; Sun, Z. Janus Nanoarchitectures: From Structural Design to Catalytic Applications. *Nano Today.* **2018**, pp 62–82.

(17) Crossley, S.; Faria, J.; Shen, M.; Resasco, D. E. Solid Nanoparticles That Catalyze Biofuel Upgrade Reactions at the Water/Oil Interface. *Science (80).* **2010**, *327* (5961), 68–72.

(18) Shi, D.; Faria, J. A.; Rownaghi, A. A.; Huhnke, R. L.; Resasco, D. E. Fischer-Tropsch Synthesis Catalyzed by Solid Nanoparticles at the Water/Oil Interface in an Emulsion System. *Energy and Fuels* **2013**, *27* (10), 6118–6124.

(19) Drexler, S.; Faria, J.; Ruiz, M. P.; Harwell, J. H.; Resasco, D. E. Amphiphilic Nanohybrid Catalysts for Reactions at the Water/Oil Interface in Subsurface Reservoirs. *Energy and Fuels* **2012**, *26* (4), 2231–2241.

(20) Kirillova, A.; Marschelke, C.; Synytska, A. Hybrid Janus Particles: Challenges and Opportunities for the Design of Active Functional Interfaces and Surfaces. *ACS Applied Materials and Interfaces*. American Chemical Society **2019**, pp 9643–9671.

(21) Kirillova, A.; Schliebe, C.; Stoychev, G.; Jakob, A.; Lang, H.; Synytska, A. Hybrid Hairy Janus Particles Decorated with Metallic Nanoparticles for Catalytic Applications. *ACS Appl. Mater. Interfaces* **2015**, *7* (38), 21224–21225.

(22) Kong, X.; Wu, C.; Feng, L.; Qu, J.; Liu, P.; Wang, X.; Zhang, X. Silica-Based Hierarchical Porous Janus Microcapsules: Construction and Support of Au Nano-Particle Catalyst Inside. *Chem. Commun.* **2017**, *53* (57), 8054–8057.

(23) Vafaeezadeh, M.; Breuninger, P.; Lösch, P.; Wilhelm, C.; Ernst, S.; Antonyuk, S.; Thiel, W. R. Janus Interphase Organic-Inorganic Hybrid Materials: Novel Water-Friendly Heterogeneous Catalysts. *ChemCatChem* **2019**, *11* (9), 2304–2312.

(24) Liu, Y.; Hu, J.; Yu, X.; Xu, X.; Gao, Y.; Li, H.; Liang, F. Preparation of Janus-Type Catalysts and Their Catalytic Performance at Emulsion Interface. *J. Colloid Interface Sci.* **2017**, *490*, 357–364.

(25) Cho, J.; Cho, J.; Kim, H.; Lim, M.; Jo, H.; Kim, H.; Min, S. J.; Rhee, H.; Kim, J. W. Janus Colloid Surfactant Catalysts for: In Situ Organic Reactions in Pickering Emulsion Microreactors. *Green Chem.* **2018**, *20* (12), 2840–2844.

(26) Adams, D. J.; Adams, S.; Melrose, J.; Weaver, A. C. Influence of Particle Surface Roughness on the Behaviour of Janus Particles at Interfaces. *Colloids Surfaces A Physicochem. Eng. Asp.* **2008**, *317* (1–3), 360–365.

(27) Park, B. J.; Brugarolas, T.; Lee, D. Janus Particles at an Oil-Water Interface. *Soft Matter* **2011**, *7* (14), 6413–6417.

(28) Hong, L.; Jiang, S.; Granick, S. Simple Method to Produce Janus Colloidal Particles in Large Quantity. *Langmuir* **2006**, *22* (23), 9495–9499.

(29) Perro, A.; Meunier, F.; Schmitt, V.; Ravaine, S. Production of Large Quantities of "Janus" Nanoparticles Using Wax-in-Water Emulsions. *Colloids Surfaces A Physicochem. Eng. Asp.* **2009**, *332* (1), 57–62.

(30) Etienne, M.; Walcarius, A. Analytical Investigation of the Chemical Reactivity and Stability of Aminopropyl-Grafted Silica in Aqueous Medium. *Talanta* **2003**, *59* (6), 1173–1188.

(31) Smith, E. A.; Chen, W. How to Prevent the Loss of Surface Functionality Derived from Aminosilanes. *Langmuir* **2008**, *24* (21), 12405–12409.

(32) Waddell, T. G.; Leyden, D. E.; DeBello, M. T. The Nature of Organosilane to Silica-Surface Bonding. *J. Am. Chem. Soc.* **1981**, *103* (18), 5303–5307.

(33) Hao, P.; Schwartz, D. K.; Medlin, J. W. Phosphonic Acid Promotion of Supported Pd Catalysts for Low Temperature Vanillin Hydrodeoxygenation in Ethanol. *Appl. Catal. A Gen.* **2018**, *561* (April), 1–6.

(34) O'Rear, D. J.; Löffler, D. G.; Boudart, M. Catalytic Hydrogenation of Cyclohexene. VI. Turnover Rate of the Gas-Phase Reaction on Unsupported Platinum Powders. *J. Catal.* **1985**, *94* (1), 225–229.

(35) Jiang, S.; Schultz, M. J.; Chen, Q.; Moore, J. S.; Granick, S. Solvent-Free Synthesis of Janus Colloidal Particles. *Langmuir* **2008**, *24* (18), 10073–10077.

(36) Aveyard, R.; Binks, B. P.; Clint, J. H. Emulsions Stabilized Solely by Colloidal Particles. *Adv. Colloid Interface Sci.* **2003**, *100–102*, 503–546.

(37) Procházková, D.; Zámostný, P.; Bejblová, M.; Červený, L.; Čejka, J. Hydrodeoxygenation of Aldehydes Catalyzed by Supported Palladium Catalysts. *Appl. Catal. A Gen.* **2007**, *332* (1), 56–64.

(38) Hao, P.; Schwartz, D. K.; Medlin, J. W. Effect of Surface Hydrophobicity of Pd/Al2O3 on Vanillin Hydrodeoxygenation in a Water/Oil System. *ACS Catal.* **2018**, *8* (12), 11165–11173.

(39) Gröger, H.; Hummel, W. Combining the "two Worlds" of Chemocatalysis and Biocatalysis towards Multi-Step One-Pot Processes in Aqueous Media. *Current Opinion in Chemical Biology.* **2014**, pp 171–179.

(40) Marr, A. C.; Liu, S. Combining Bio- and Chemo-Catalysis : From Enzymes to Cells , from Petroleum to Biomass. *Trends Biotechnol.* **2011**, *29* (5), 199–204.

(41) Schwartz, T. J.; Shanks, B. H.; Dumesic, J. A. Direct Coupling Chemical and Biological Catalysis : A Flexible Paradigm for Producing Biobased Chemicals. *Curr. Opin. Biotechnol.* **2016**, *38*, 54–62.

(42) Schmidt, S.; Castiglione, K.; Kourist, R. Overcoming the Incompatibility Challenge in Chemoenzymatic and Multi-Catalytic Cascade Reactions. *Chemistry - A European Journal.* **2018**, pp 1755–1768.

(43) van Oers, M. C. M.; Rutjes, F. P. J. T.; Van Hest, J. C. M. Cascade Reactions in Nanoreactors. *Curr. Opin. Biotechnol.* **2014**, *28*, 10–16.

(44) Liu, T. Z.; Lee, S. D.; Bhatnagar, R. S. Toxicity of Palladium. *Toxicol. Lett.* **1979**, *4* (6), 469–473.

(45) Chen, Z.; Wan, C. Biological Valorization Strategies for Converting Lignin into Fuels and Chemicals. *Renewable and Sustainable Energy Reviews.* Elsevier Ltd **2017**, pp 610–621.

(46) Chen, B. Y. Understanding Decolorization Characteristics of Reactive Azo Dyes by Pseudomonas Luteola: Toxicity and Kinetics. *Process Biochem.* **2002**, *38* (3), 437–446.

(47) Fu, Y.; Xu, P.; Huang, D.; Zeng, G.; Lai, C.; Qin, L.; Li, B.; He, J.; Yi, H.; Cheng, M.; et al. Au Nanoparticles Decorated on Activated Coke via a Facile Preparation for Efficient Catalytic Reduction of Nitrophenols and Azo Dyes. *Appl. Surf. Sci.* **2019**, *473*, 578–588.

**Graphical abstract**

Amphiphilic surface chemistry
Regioselective metal deposition

Selective oil-phase catalysis